Inorg. Chem. **2006**, *45*, 1277−1288

Mono-, Di-, and Oligonuclear Complexes of Cu^{II} Ions and *p*-Hydroquinone Ligands: Syntheses, Electrochemical Properties, and Magnetic Behavior

GUnter Margraf,[†] Tonia Kretz,[†] Fabrizia Fabrizi de Biani,[‡] Franco Laschi,[‡] Serena Losi,[‡] Piero Zanello,*[,‡] Jan W. Bats,[§] Bernd Wolf,[||] Katarina Remović-Langer,[||] Michael Lang,[||] Andrei Prokofiev,[||] Wolf Assmus,[||] Hans-Wolfram Lerner,[†] and Matthias Wagner*[,†]

Institut für Anorganische Chemie and Institut für Organische Chemie, J.W. Goethe-Universität Frankfurt, Marie-Curie-Strasse 11, D-60439 Frankfurt (Main), Germany, Dipartimento di Chimica dell'Università, Via Aldo Moro, I-53100 Siena, Italy, and Physikalisches Institut, J.W. Goethe-Universität Frankfurt, Max-von-Laue-Strasse 1, 60438 Frankfurt (Main), Germany

Received June 22, 2005

Four highly soluble square-planar Cu^{II} and Ni^{II} complexes of siloxy-salens (**2SiCu**, **2SiNi**) and hydroxy-salens (**2Cu**, **2Ni**) have been synthesized. An X-ray crystal structure analysis was performed on **2SiCu**, **2SiNi**, and **2Ni.** The compounds have been investigated by cyclic voltammetry, UV−vis−NIR spectroelectrochemistry, and EPR spectroscopy. According to these results, the monooxidized species $[\mathbf{2SiCu}]^+$ and $[\mathbf{2SiNi}]^+$ are to be classified as Robin−Day class II and III systems, respectively. Magnetic measurements on the dinuclear (PMDTA)Cu^{II} complex $\mathbf{1Cu_2 \cdot (PF_6)_2}$ with deprotonated 1,4-dihydroxy-2,5-bis(pyrazol-1-yl)-benzene (**1**) linker revealed antiferromagnetic coupling between the two Cu^{II} ions thereby resulting in an isolated dimer compound. Coordination polymers $[\mathbf{1Cu}]_n(\mathbf{H_2O})_{2n}$ of Cu^{II} ions and bridging *p*-hydroquinone linkers were obtained from $CuSO_4 \cdot 5H_2O$ and 1,4-dihydroxy-2,5-bis(pyrazol-1-yl)benzene. X-ray crystallography revealed linear chains running along the crystallographic *a*-direction and stacked along the *b*-axis. Within these chains, the Cu^{II} ions are coordinated by two pyrazolyl nitrogen atoms and two *p*-hydroquinone oxygen atoms in a square-planar fashion.

Introduction

Cooperative magnetic phenomena in low-dimensional spin systems continue to be of great interest because the behavior of, for example, linear spin chains differs greatly from the magnetic properties of materials in which spin−spin coupling occurs in all three dimensions.[1−4] Starting from Cu^{II} ions and bridging 1,4-dihydroxy-2,5-bis(pyrazol-1-yl)benzene ligands[5−7] (**1**, Figure 1), our group has recently prepared the coordination polymer $[\mathbf{1Cu}]_n$ (Figure 1).[8] The structure of the purple material was determined by high-resolution X-ray powder diffraction using the method of simulated annealing. The crystal lattice of $[\mathbf{1Cu}]_n$ consists of largely isolated linear chains featuring Cu^{II} ions coordinated in a square-planar fashion by two nitrogen atoms and two negatively charged oxygen donors (shortest interchain Cu···Cu distance: 5.2 Å).[8] By means of magnetic measurements as a function of temperature and magnetic field, $[\mathbf{1Cu}]_n$ was shown to behave as a homogeneous antiferromagnetic $S = {}^1/_2$ Heisenberg spin chain with a moderate exchange-coupling constant J/k_B of −21.5 K. The acoustic and magnetic anomalies of $[\mathbf{1Cu}]_n$

* E-mail: zanello@unisi.it (P.Z.); Matthias.Wagner@chemie.uni-frankfurt.de (M.W.).
[†] Institut für Anorganische Chemie, J.W. Goethe-Universität Frankfurt.
[‡] Dipartimento di Chimica dell'Università.
[§] Institut für Organische Chemie, J.W. Goethe-Universität Frankfurt.
[||] Physikalisches Institut, J.W. Goethe-Universität Frankfurt.

(1) Mermin, N. D.; Wagner, H. *Phys. Rev. Lett.* **1966**, *17*, 1133.
(2) Kahn, O. *Molecular Magnetism*; VCH: New York, 1993.
(3) Lueken, H. *Magnetochemie*; Teubner: Stuttgart, 1999.
(4) *Quantum Magnetism*, *Lect. Notes Phys*; Schollwöck, U., Richter, J., Farnell, D. J. J., Bishop, R. F., Eds.; Springer: Berlin, 2004; Vol. 645.
(5) Gauss, W.; Heitzer, H.; Petersen, S. *Liebigs Ann. Chem.* **1972**, *764*, 131.
(6) Catalán, J.; Fabero, F.; Guijarro, M. S.; Claramunt, R. M.; Santa Maria, M. D.; Foces-Foces, M. C.; Cano, F. H.; Elguero, J.; Sastre, R. *J. Am. Chem. Soc.* **1990**, *112*, 747.
(7) Ballesteros, P.; Claramunt, R. M.; Escolástico, C.; Santa Maria, M. D.; Elguero, J. *J. Org. Chem.* **1992**, *57*, 1873.
(8) Dinnebier, R.; Lerner, H.-W.; Ding, L.; Shankland, K.; David, W. I. F.; Stephens, P. W.; Wagner, M. *Z. Anorg. Allg. Chem.* **2002**, *628*, 310.

10.1021/ic051016z CCC: $33.50
Published on Web 01/07/2006

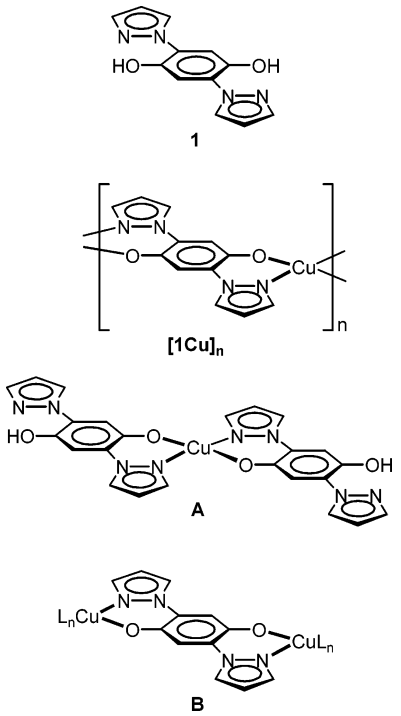

Figure 1. The *p*-hydroquinone-based bridging ligand **1**, the corresponding Cu^{II} coordination polymer $[\mathbf{1Cu}]_n$, and the model complexes **A** and **B** representing two different fragments of the polymer structure.

near the saturation field have also been studied and results are reported elsewhere.[9,10]

To us, *p*-hydroquinone ligands such as **1** appeared to be particularly attractive for the preparation of coordination polymer-based magnetic materials, because **1** can adopt three different stable oxidation states, one of which (the semiquinone state) is paramagnetic. It should therefore be possible to modify the magnetic properties of $[\mathbf{1Cu}]_n$ electrochemically, because the value of the Cu^{II}/Cu^{II} exchange-coupling constant *J* can be expected to depend critically on the electron density of the bridging ligand's π system. Moreover, additional unpaired spins may be injected into the chain simply by partial oxidation of the organic building blocks to their semiquinone state. Prior to magnetic measurements on electrochemically doped $[\mathbf{1Cu}]_n$, the redox chemistry of this material needs to be fully explored. Because electrochemical data of the actual polymer $[\mathbf{1Cu}]_n$ are hard to obtain due to its low solubility in all common organic solvents, we decided to start with an investigation of soluble model systems **A** and **B** (Figure 1). These compounds should already provide important information about the relevant redox potentials and the degree of electronic communication between the *p*-hydroquinone unit(s) and the Cu^{II} ion(s). Thus, the purpose of this paper is to report on the synthesis, the structural characterization, and a detailed electrochemical investigation of selected **A**- and **B**-type compounds. (Note: In the literature, only very few metal complexes of **1** or related ligands have been reported.[8,11−15])

Results and Discussion

Syntheses and Spectroscopy. Our attempts to prepare **A** (Figure 1) by treating 2 equiv of **1** with 1 equiv of an appropriate Cu^{II} salt failed, because they always resulted in the precipitation of insoluble (likely polymeric) material irrespective of the reaction conditions applied. The same was true when the truncated ligand 1,4-dihydroxy-2-(pyrazol-1-yl)-benzene[6,7] was employed, even though this compound possesses only one chelating pyrazolyl sidearm. It was therefore necessary to modify the initial target structure substantially and to switch from **1** to the alternative *p*-hydroquinone-containing ligand **2Si** (Scheme 1). Various chiral derivatives of **2Si** have already been described by Jacobsen et al., and the corresponding transition metal complexes proved to be monomeric and highly soluble.[16] Moreover, by comparing the electrochemical data of the silylated complexes with those of the analogous deprotected derivatives, an assignment of relevant redox transitions may be facilitated. Our synthesis of **2Si**, which uses 2 equiv of 2-hydroxy-3-*t*-butyl-5-(triisopropylsiloxy)benzaldehyde and 1 equiv of ethylenediamine, follows the general route developed by Jacobsen's group (Scheme 1).[16] Treatment of **2Si** with 1 equiv of Cu^{II} acetate in THF at room temperature (rt) resulted in the clean formation of **2SiCu**. Desilylation of **2SiCu** to the free hydroxy derivative **2Cu** was achieved by addition of $[NBu_4]F\cdot 3H_2O$. Because we have not been able to grow single crystals of **2Cu**, the unsubstituted parent compound **3Cu** was prepared in a one-pot reaction from 2,5-dihydroxybenzaldehyde, ethylenediamine, and Cu^{II} acetate. In contrast to **2Cu**, **3Cu** readily crystallized from DMF at rt (**3Cu**·DMF). To be able to compare the electrochemical behavior of square-planar Cu^{II} complexes (electron configuration: d^9) with the redox properties of analogous square-planar d^8-metal compounds, we also prepared the Ni^{II} complexes **2SiNi** and **2Ni**. In both cases, the synthesis followed the reaction scheme outlined for **2SiCu** and **2Cu**.

The preparation of dinuclear complexes **B** (Figure 1) is severely hampered by the fact that the low solubility of $[\mathbf{1Cu}]_n$ tends to shift the reaction equilibrium toward polymer formation. Thus, a systematic screening of possible mononuclear Cu^{II} precursor complexes and Brønstedt bases for hydroquinone deprotonation was required (cf. Supporting Information). Finally, the Cu^{II} complex $[Cu(PMDTA)(Me_2CO)Cl]PF_6$ (PMDTA = *N*,*N*′,*N*″,*N*″-pentamethyldiethylenetriamine) and thallium ethoxide (TlOEt) turned out to be the reagents of choice, likely because the high lattice

(9) Wolf, B.; Zherlitsyn, S.; Lüthi, B.; Harrison, N.; Löw, U.; Pashchenko, V.; Lang, M.; Margraf, G.; Lerner, H.-W.; Dahlmann, E.; Ritter, F.; Assmus, W.; Wagner, M. *Phys. Rev. B* **2004**, *69*, 092403.
(10) Wolf, B.; Brühl, A.; Magerkurth, J.; Zherlitsyn, S.; Pashchenko, V.; Brendel, B.; Margraf, G.; Lerner, H.-W.; Wagner, M.; Lüthi, B.; Lang, M. *J. Magn. Magn. Mater.* **2005**, *290*−*291*, 411.
(11) Ernst, S.; Hänel, P.; Jordanov, J.; Kaim, W.; Kasack, V.; Roth, E. *J. Am. Chem. Soc.* **1989**, *111*, 1733.
(12) Dei, A.; Gatteschi, D.; Pardi, L. *Inorg. Chem.* **1990**, *29*, 1442.
(13) Cornago, P.; Escolástico, C.; Santa María, M. D.; Claramunt, R. M.; Carmona, D.; Esteban, M.; Oro, L. A.; Foces-Foces, C.; Llamas-Saiz, A. L.; Elguero, J. *J. Organomet. Chem.* **1994**, *467*, 293.
(14) Keyes, T. E.; Jayaweera, P. M.; McGarvey, J. J.; Vos, J. G. *J. Chem. Soc., Dalton Trans.* **1997**, 1627.
(15) Keyes, T. E.; Forster, R. J.; Jayaweera, P. M.; Coates, C. G.; McGarvey, J. J.; Vos, J. G. *Inorg. Chem.* **1998**, *37*, 5925.
(16) Ready, J. M.; Jacobsen, E. N. *J. Am. Chem. Soc.* **2001**, *123*, 2687.

Scheme 1. Syntheses of the Disilylated *p*-Hydroquinone Ligand **2Si** and of its Cu^{II} and Ni^{II} Complexes **2SiCu** and **2SiNi**, Deprotection of **2SiCu** and **2SiNi** to the Free *p*-Hydroquinone Complexes **2Cu** and **2Ni**, and One-Pot Synthesis of the Unsubstituted *p*-Hydroquinone−Cu^{II} Complex **3Cu**[a]

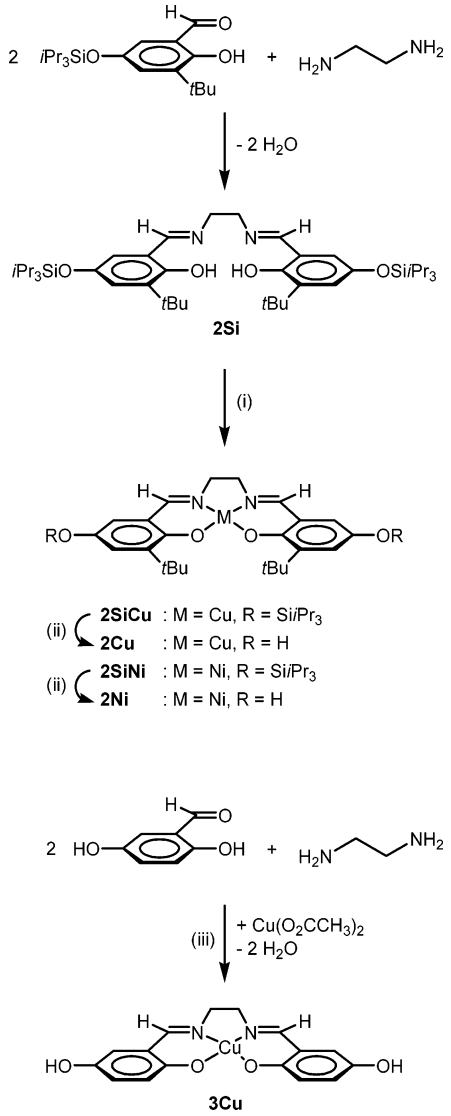

[a] (i) **2SiCu**: + $Cu(O_2CCH_3)_2$, THF, 15 h, rt; **2SiNi**: + $Ni(O_2CCH_3)_2$, THF/CH_3OH, 15 h, rt. (ii) + $[NBu_4]F{\cdot}3H_2O$, THF, 15 h, −78 °C to rt. (iii) THF, 18 h, reflux.

energy of thallium chloride is crucial to drive the substitution reaction between $[Cu(PMDTA)(Me_2CO)Cl]PF_6$ and **1** to completion. By this method, $\mathbf{1Cu_2{\cdot}(PF_6)_2}$ was prepared in 53% yield. An analysis of the material with the help of total-reflection X-ray fluorescence (TXRF) spectroscopy revealed the presence of substantial amounts of thallium, but no contamination with chloride ions. We therefore conclude that Tl^I ions are to some extent able to compete successfully with the Cu^{II} ions for the coordination sites of ligand **1**. To get a more quantitative picture, we prepared a derivative of **1** with bromine substituents at the 4-position of its pyrazolyl sidearms (**1Br**) and added $[Cu(PMDTA)(Me_2CO)Cl]PF_6$/TlOEt following the same synthesis protocol as described above for the preparation of $\mathbf{1Cu_2{\cdot}(PF_6)_2}$ (Scheme 2). TXRF analysis of the resulting compound $\mathbf{1BrCu_2{\cdot}(PF_6)_2}$ gave a ratio Br:Cu:Tl of 2:1.65:0.35, indicating about 20% of all

Scheme 2. Synthesis of the *p*-Hydroquinone-Bridged Dinuclear Cu^{II} Complexes $\mathbf{1Cu_2{\cdot}(PF_6)_2}$ and $\mathbf{1BrCu_2{\cdot}(PF_6)_2}$[a]

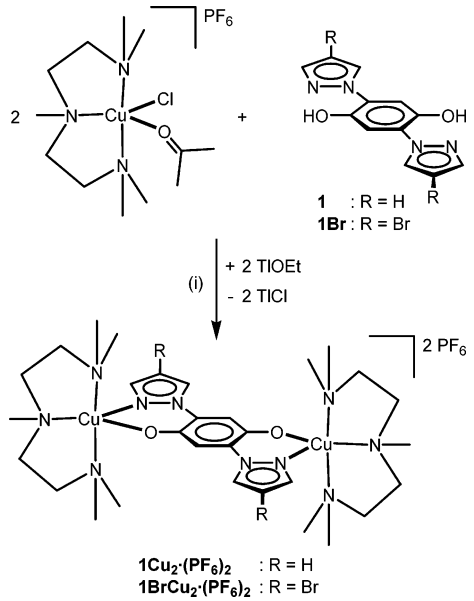

[a] (i) EtOH, 1 h, rt.

Cu^{II} coordination sites to be occupied by Tl^I ions. Attempts to purify $\mathbf{1Cu_2{\cdot}(PF_6)_2}$ by column chromatography or HPLC failed because the compound turned out to be rather labile. Initially purple solutions of $\mathbf{1Cu_2{\cdot}(PF_6)_2}$ in methanol or DMSO, prepared and stored under an inert gas atmosphere, turned green within a few minutes. Under similar conditions, an acetonitrile solution of $\mathbf{1Cu_2{\cdot}(PF_6)_2}$ gradually lost its color while a dark precipitate formed. Mass spectra of the mixtures obtained after decomposition suggest $\mathbf{1Cu_2{\cdot}(PF_6)_2}$ to have lost one of its $[Cu(PMDTA)]^{2+}$ moieties. Nevertheless, we succeeded in growing X-ray quality crystals of $\mathbf{1Cu_2{\cdot}(PF_6)_2}$ by gas-phase diffusion of diethyl ether into a DMF solution of the crude material. Because the amount of pure crystalline $\mathbf{1Cu_2{\cdot}(PF_6)_2}$ was very small, an investigation of its electrochemical properties was not possible.

The growth of single-crystalline $[\mathbf{1Cu}]_n$ proved to be a major challenge. One problem is the strong binding anisotropy in the crystal lattice since bonds along the coordination polymer chains are much stronger than any interchain interactions along the other two crystal axes. After numerous efforts, we finally obtained few very small single-crystals of the desired coordination polymer employing the starting materials $CuSO_4{\cdot}5H_2O$ and **1** in aqueous ammonia. The material turned out to be a pseudopolymorph of the previously investigated $[\mathbf{1Cu}]_n$ because it contained two water molecules in the unit cell ($\mathbf{[1Cu]_n(H_2O)_{2n}}$).

The ^1H and ^{13}C NMR signals of **2Si** appear in the expected regions and therefore do not merit further discussion. The largest changes observed in the ^1H NMR spectrum upon complexation of **2Si** with a Ni^{II} ion come upon the imine and ethylene proton resonances, which are shifted to higher field by 0.92 ppm [**2Si**, $\delta(^1H) = 8.28$; **2SiNi**, $\delta(^1H) = 7.36$] and 0.62 ppm [**2Si**, $\delta(^1H) = 3.89$; **2SiNi**, $\delta(^1H) = 3.27$], respectively. A similar effect is observed for the ^{13}C NMR signal of the imine carbon atom, which is significantly more shielded in **2SiNi** [$\delta(^{13}C) = 161.4$] than in **2Si** [$\delta(^{13}C) =$

Table 1. Crystallographic Data for $\mathbf{1Cu_2{\cdot}(PF_6)_2}$, and $[\mathbf{1Cu}]_n\mathbf{(H_2O)_{2n}}$

	$1Cu_2{\cdot}(PF_6)_2$	$[1Cu]_n(H_2O)_{2n}$
formula	$C_{30}H_{54}Cu_2F_{12}N_{10}O_2P_2$	$C_{12}H_{12}CuN_4O_4$
fw	1003.85	339.80
color, shape	black, rod	brown, block
crystal size (mm^3)	0.60 × 0.22 × 0.14	0.12 × 0.10 × 0.03
temp (K)	156(2)	150(2)
radiation	Mo Kα, 0.71073 Å	Mo Kα, 0.71073 Å
cryst syst	monoclinic	monoclinic
space group	$P2_1/c$	$P2_1/n$
a (Å)	7.6587(8)	8.3167(13)
b (Å)	20.460(3)	4.8505(7)
c (Å)	14.015(3)	15.561(2)
α (°)	90	90
β (°)	105.026(15)	94.108(7)
γ (°)	90	90
V ($Å^3$)	2121.1(6)	626.10(16)
Z	2	2
D_{calcd} (g cm^{-3})	1.572	1.802
$F(000)$	1032	346
μ (mm^{-1})	1.173	1.768
$2\theta_{max}$ (°)	64.46	55.26
no. of reflns collected	27051	3065
no. of indep reflns (R_{int})	6430 (0.0303)	1285 (0.1095)
no. of reflns obsd ($I > 2\sigma(I)$)	5523	635
no. of data/restraints/params	6430/0/283	1285/2/106
GOF on F^2	1.192	0.922
R1, wR2 ($I > 2\sigma(I)$)	0.0353, 0.0785	0.0622, 0.1047
R1, wR2 (all data)	0.0451, 0.0820	0.1578, 0.1270
largest diff peak and hole (e $Å^{-3}$)	0.477/−0.504	0.562/−0.929

167.0]. In the case of the ethylene carbon resonances, however, the corresponding chemical shift values are almost the same for the free ligand and its Ni^{II} complex [**2Si**, $\delta(^{13}C) = 59.7$; **2SiNi**, $\delta(^{13}C) = 58.4$]. As an experimental probe for the charge density distribution within a molecule, ^{13}C NMR spectroscopy provides a more reliable diagnostic tool than ^1H NMR spectroscopy, because proton shift values may be greatly influenced by magnetic anisotropy effects.[17] Ni^{II} binding thus apparently leads to some accumulation of negative charge on the imine fragment, whereas the electron density on the ethylene bridge is merely unchanged. The ^1H and ^{13}C NMR spectra of **2Ni** show no signals assignable to *i*-Pr_3Si groups. Instead, a resonance at 7.69 ppm (s, 2H) appears in the proton spectrum testifying to the presence of free hydroxyl groups.

X-ray Crystal Structure Analyses. Details of the X-ray crystal structure analyses of $\mathbf{1Cu_2{\cdot}(PF_6)_2}$ and $[\mathbf{1Cu}]_n\mathbf{(H_2O)_{2n}}$ are summarized in Table 1 (for **2Si**, **2SiCu**, **3Cu**·DMF, **2SiNi**, and **2Ni**·$(MeOH)_2$ this information, together with plots of the molecular structures and a compilation of selected bond lengths, bond angles, and torsion angles, can be found in the Supporting Information: Table 1S, Figures 1S−5S).

$\mathbf{1Cu_2{\cdot}(PF_6)_2}$ crystallizes from diethyl ether/DMF in the monoclinic space group $P2_1/c$ (Figure 2). In the solid state, the molecules are centrosymmetric with a crystallographic inversion center located at the midpoint of the central benzene ring. The Cu^{II} ions have approximately square-pyramidal coordination geometry. The equatorial positions are occupied by the donor atoms O, N(3), N(4), and N(5) (Cu−O = 1.915(1) Å, Cu−N(3) = 2.101(2) Å, Cu−N(4) = 2.052(1) Å, Cu−N(5) = 2.080(1) Å), while the pyrazolyl sidearm is located at the axial position and features a

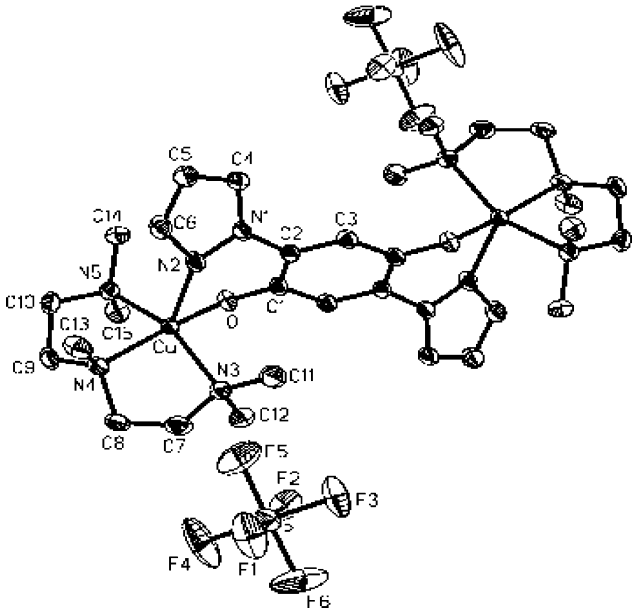

Figure 2. Molecular structure of $\mathbf{1Cu_2{\cdot}(PF_6)_2}$ in the solid state, with thermal ellipsoids at the 50% probability level. H atoms have been omitted for clarity. Selected bond lengths (Å), bond angles (deg), and torsion angles (deg): Cu−O 1.915(1), Cu−N(2) 2.271(2), Cu−N(3) 2.101(2), Cu−N(4) 2.052(1), Cu−N(5) 2.080(1), C(1)−C(2) 1.413(2), C(1)−C(3)#1 1.404(2), C(2)−C(3) 1.389(2); O−Cu−N(2) 88.4(1), O−Cu−N(3) 96.5(1), O−Cu−N(4) 164.0(1), O−Cu−N(5) 87.4(1), N(2)−Cu−N(3) 101.9(1), N(2)−Cu−N(4) 106.8(1), N(2)−Cu−N(5) 102.0(1), N(3)−Cu−N(4) 85.4(1), N(3)−Cu−N(5) 155.8(1), N(4)−Cu−N(5) 84.7(1), Cu−O−C(1) 121.3(1), Cu−N(2)−N(1) 114.9(1), O−C(1)−C(2) 124.0(1), O−C(1)−C(3)#1 120.4(1), C(2)−C(1)−C(3)#1 115.6(1); Cu−O−C(1)−C(2) −48.5(2), Cu−N(2)−N(1)−C(2) −35.4(2), N(1)−N(2)−Cu−N(3) 91.8(1), N(1)−N(2)−Cu−N(4) −179.5(1), N(1)−N(2)−Cu−N(5) −91.5(1), N(3)−C(7)−C(8)−N(4) −55.7(2), N(4)−C(9)−C(10)−N(5) 53.1(2). Symmetry transformations used to generate equivalent atoms: #1, $-x + 1$, $-y + 1$, $-z$.

significantly longer bond Cu−N(2) = 2.271(2) Å. The Cu ion deviates by 0.34 Å from the best plane through O, N(3), N(4), and N(5) in the direction toward the center of the pyramid. The angle between the planes of the phenylene ring and the pyrazolyl substituents is 43.9°. The Cu^{II} coordination polymer $[\mathbf{1Cu}]_n\mathbf{(H_2O)_{2n}}$ (monoclinic, $P2_1/n$; Figure 3) forms chains along the crystallographic *a*-direction, which are stacked along the *b*-axis (shortest intermolecular Cu···Cu contact, 4.851(1) Å; cf. $[\mathbf{1Cu}]_n$, 5.2 Å; for a perspective view of the packing of the chains in a projection along the *b*-axis see the Supporting Information, Figure 6S).[18] The Cu^{II} ion lies on a crystallographic inversion center. A second crystallographically generated inversion center is located at the midpoint of the central phenylene ring. The Cu^{II} ion is bonded to two pyrazolyl nitrogen donors (Cu−N(2) = 1.952(5) Å) and two *p*-hydroquinone moieties (Cu−O(1) = 1.901(3) Å) in a square-planar fashion. Its position deviates by 0.91 Å from the best plane through the central phenylene ring and 0.14 Å from the best plane through the pyrazolyl anchor group. The dihedral angle between the benzene ring and its pyrazolyl substituents amounts to 20.7°. The water molecules are interconnected via hydrogen bonds thereby forming zigzag chains along the crystallographic *b*-direction. Each water molecule donates a hydrogen bond to a ring

(17) Hesse, M.; Meier, H.; Zeeh, B. *Spektroskopische Methoden in der Organischen Chemie*; Thieme: Stuttgart, 1987.

(18) Manfredotti, A. G.; Guastini, C. *Acta Crystallogr., Sect. C* **1983**, *39*, 863.

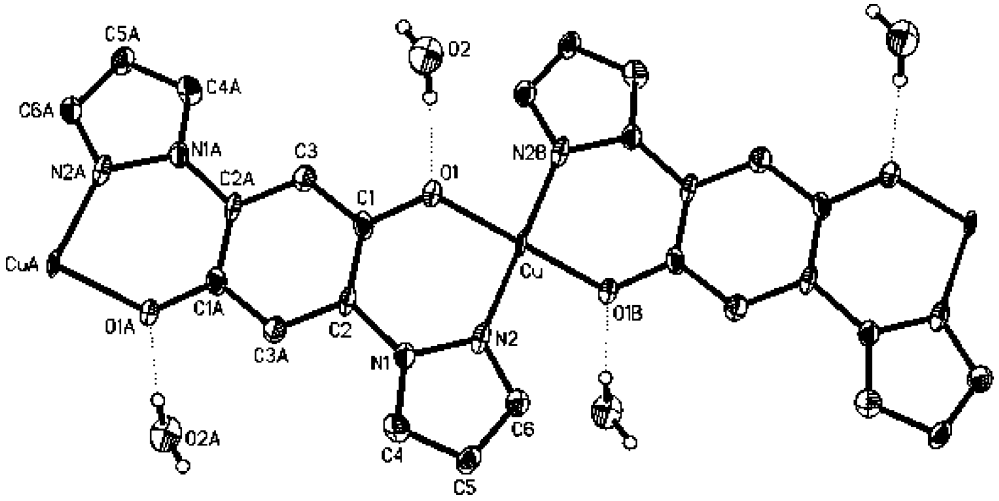

Figure 3. Molecular structure of $[\mathbf{1Cu}]_n(\mathbf{H_2O})_{2n}$ in the solid state, with thermal ellipsoids at the 50% probability level. Some H atoms have been omitted for clarity. Selected bond lengths (Å) and angles (deg): Cu−O(1) 1.901(3), Cu−N(2) 1.952(5), O(1)−Cu−O(1)#1 180.0, O(1)−Cu−N(2) 89.2(2), O(1)−Cu−N(2)#1 90.8(2), N(2)−Cu−N(2)#1 180.0, Cu−N(2)−N(1) 127.6(4). Symmetry transformations used to generate equivalent atoms: #1, $-x, -y, -z$; #2, $-x - 1, -y, -z$.

oxygen atom (H(2)···O(1) = 1.87(2) Å, O(2)−H(2)···O(1) = 170(7)°) and a second bond to a neighboring water molecule. It is important to note that the occupance factor of the Cu ion refined to 0.836(5) only. This leads to the conclusion that each sixth metal atom position is not occupied by Cu^{II} but rather by two protons (EDX measurement on the actual crystal that was used for X-ray diffraction showed that the crystal contained no heavy elements other than C, N, O, and Cu). No distortion of the structure due to the Cu^{II} vacancies was observed. This is not too surprising if one considers the coordination chemistry of porphyrin molecules which provide a ligand framework with a geometry similar to that established by the two ligands **1** in $[\mathbf{1Cu}]_n(\mathbf{H_2O})_{2n}$. The extremely rigid porphyrin macrocycles also exist both in the free form and as metal complexes.

Magnetic Measurements. Magnetic characterization measurements on the dinuclear Cu^{II} complex $\mathbf{1Cu_2{\cdot}(PF_6)_2}$ were carried out to determine the degree of spin−spin coupling via the *p*-hydroquinone bridge. For comparison, the mononuclear Cu^{II} complexes **2SiCu** and **3Cu**·DMF were also investigated (cf. Supporting Information). Figure 4 shows the temperature dependence of the molar susceptibility $\chi_{mol}(T)$ for the dinuclear complex $\mathbf{1Cu_2{\cdot}(PF_6)_2}$. The data have been corrected for a temperature-independent diamagnetic contribution and a Curie contribution which results from about 30% uncoupled $S = {}^1/_2$ Cu^{II} spins. The latter can be clearly identified also in the magnetization measurements up to 5 T. This Curie contribution is most likely due to the fact that the sample was contaminated with a Cu^{II}/Tl^{I} heterodinuclear compound as explained above. The so-derived $\chi_{mol}(T)$ of $\mathbf{1Cu_2{\cdot}(PF_6)_2}$ increases continuously from 290 K down to about 40 K, below which it rapidly drops. For temperatures around 7 K, the susceptibility of $\mathbf{1Cu_2{\cdot}(PF_6)_2}$ vanishes as expected for a system of isolated antiferromagnetically coupled Cu^{II} dimers after the diamagnetic core contributions have been subtracted.[19] Employing a fit according to the Bleaney−Bowers equation based on a Hamiltonian $H = -J\Sigma_{[i,j]}S_i{\cdot}S_j$ (straight line in Figure 4), a good description of the experimental data is obtained yielding an intradimer exchange coupling constant of $J/k_B = -63 \pm 5$ K.[2,20]

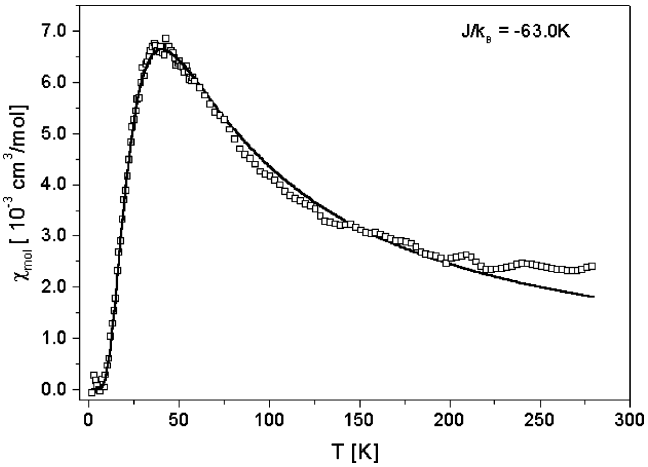

Figure 4. Molar magnetic susceptibility of $\mathbf{1Cu_2{\cdot}(PF_6)_2}$ as a function of temperature after subtracting the diamagnetic core contribution and a Curie contribution, which results from about 30% uncoupled $S = {}^1/_2$ Cu^{II} spins. The straight line is a fit according to the Bleaney−Bowers equation.

Electrochemical and Joint Spectroelectrochemical Investigation. Cyclic Voltammetric Measurements. The formal electrode potentials of all compounds under investigation here are compiled in Table 2. To rationalize the redox behavior of complexes **2SiCu** and **2SiNi** it is useful to look at the voltammetric profile of the free ligand **2Si** first (CH_2Cl_2 solution). Ligand **2Si** exhibits two oxidation processes with features of chemical reversibility on the cyclic voltammetric time scale which we assign to the *p*-hydroquinone/*p*-semiquinone passage of each quinoid fragment. Further oxidation to the respective quinone state is irreversible, likely because both the OH protons and the silyl groups are released in the course of the reaction (a plot of the cyclic

(19) Johnston, D. C.; Kremer, R. K.; Troyer, M.; Wang, X.; Klümper, A.; Bud'ko, S. L.; Panchula, A. F.; Canfield, P. C. *Phys. Rev. B* **2000**, *61*, 9558.

(20) Bleaney, B.; Bowers, K. D. *Proc. R. Soc. London* **1952**, *A11*, 303.

Table 2. Formal Electrode Potentials $E°'$ (V, vs. SCE) and Peak-to-Peak Separations ΔE_p (mV) for the Anodic Processes Exhibited by the Free Ligands **2Si** and **2H** and the Complexes **2SiCu**, **2SiNi**, **2Cu**, and **2Ni**

	$E°(0/+)$	ΔE_p[a]	$E°(+/2+)$	ΔE_p[a]
2Si	+0.74[b]		+0.90	
2SiCu	+0.66	75	+0.89	75
2SiNi	+0.61	80	+1.01	80
2H	+0.60[c]		+0.78[c]	
2Cu	+0.55	66	+0.80[d]	80
2Ni	+0.58[c]		+0.76[c]	

[a] Measured at 0.2 V s^{-1}. [b] From OSQW. [c] Peak potential value for irreversible processes. [d] Two-electron process.

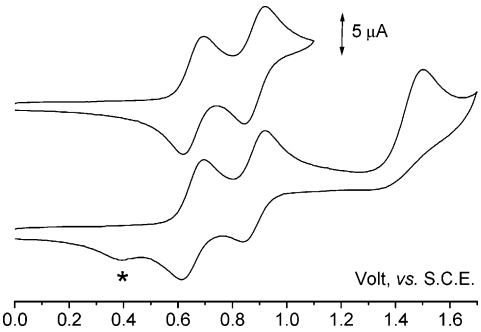

Figure 5. Cyclic voltammograms of **2SiCu** (0.8×10^{-3} mol L^{-1}) recorded at a platinum electrode in CH_2Cl_2 solution. $[NBu_4][PF_6]$ (0.2 mol L^{-1}) was used as supporting electrolyte. Scan rate 0.05 V s^{-1}.

voltammogram of **2Si** is included in the Supporting Information). A similar picture holds for the desilylated analogue **2H** apart from the fact that here all oxidation processes are irreversible.

Let us now pass to the metal complexes **2SiCu** and **2SiNi** of ligand **2Si**. Figure 5 illustrates the redox behavior of **2SiCu** in CH_2Cl_2 solution (a plot of the cyclic voltammogram of **2SiNi**, which is qualitatively similar to that of **2SiCu**, is included in the Supporting Information). Also in the cases of **2SiCu** and **2SiNi**, two oxidation processes with features of chemical reversibility on the cyclic voltammetric time scale precede a further irreversible oxidation. A spurious (starred) peak at about +0.40 V appears in the back scan after traversing the most anodic process. Moreover, **2SiCu** undergoes an irreversible reduction process at $E_p = -1.60$ V, not shown in Figure 5. The redox properties of the nonsilylated analogues **2M** (M = Cu, Ni) are strongly reminiscent of those of the complexes **2SiM**, but for some details which will be discussed below. Electrochemical data and an EPR spectroscopical investigation of **3Cu** have already been published elsewhere.[21,22] For both the **2SiM** derivatives, controlled potential coulometry in correspondence to the first anodic process consumes one electron per molecule. As a consequence, the original green solutions turn brown. Such exhaustively one-electron oxidized solutions give rise to cyclic voltammetric profiles quite complementary to the original ones, thus indicating the monocations $[\mathbf{2SiCu}]^+$ and $[\mathbf{2SiNi}]^+$ to be stable on the long time scale of

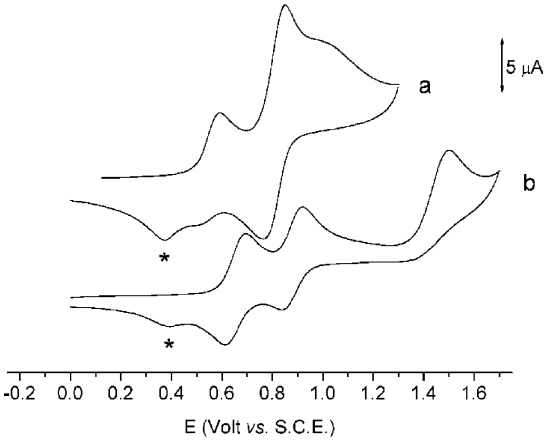

Figure 6. Cyclic voltammograms recorded at a platinum electrode in CH_2Cl_2 solutions of: (a) **2Cu** (1.2×10^{-3} mol L^{-1}); (b) **2SiCu** (0.8×10^{-3} mol L^{-1}). $[NBu_4][PF_6]$ (0.2 mol L^{-1}) was used as supporting electrolyte. Scan rate 0.2 V s^{-1}.

macroelectrolysis. Although on the time scale of cyclic voltammetry the second oxidation of **2SiCu** and **2SiNi** appears as a one-electron transition, controlled potential coulometry in correspondence to this anodic process consumes two electrons per molecule in both cases. Moreover, the resulting green-brown solution affords a cyclic voltammetric profile no more attributable to the original complex. Therefore, the second electron removal involves an E_1CE_2 mechanism ($E_2 < E_1$), which means that, after the initial formation of the semiquinone on both halves of the ligand, a new redox-active product arises which is also oxidized at the working potential. This new species looks to be related to the original complex in that it undergoes two reductions, the first of which corresponds to the $[\mathbf{2SiM}]^+/\mathbf{2SiM}$ change, while the second occurs in correspondence to the spurious peak previously noted. We conclude that, on the long time scale of exhaustive electrolysis at an electrode potential of about +1 V, the formation of two semiquinone halves is followed by a chemical reaction giving the same product as observed on the short time scale of cyclic voltammetry when the sweep was taken far into the anodic regime (i.e., up to +1.7 V). As mentioned before, a possible mechanism for the formation of the new species involves cleavage of the O−Si bonds. This hypothesis is indirectly supported by a comparison of the redox behavior of the couples **2M**/**2SiM** (M = Ni, Cu). As an example, Figure 6 illustrates the cyclic voltammograms of **2Cu** (a) and **2SiCu** (b) in CH_2Cl_2 solution. Apart from the fact that for **2Cu** the two-electron nature of the second oxidation is clearly visible even on the cyclic voltammetric time scale, it is to be noted that the spurious starred peak observed in the back scan is the same in both derivatives thereby suggesting the same decomposition product to be formed. Thus, the following conclusions may be drawn: (i) the fact that the two *p*-hydroquinone/*p*-semiquinone transitions are less reversible for **2M** than for **2SiM** may be explained by the easier loss of OH-protons as compared to the liberation of silyl groups; (ii) the inner metal complex core is maintained during the electrochemical processes. Electrochemical investigations of the dinuclear Cu^{II} complex $\mathbf{1Cu_2{\cdot}(PF_6)_2}$ are affected by its contamination

(21) Lamour, E.; Routier, S.; Bernier, J.-L.; Catteau, J.-P.; Bailly, C.; Vezin, H. *J. Am. Chem. Soc.* **1999**, *121*, 1862.
(22) Charles, E. H.; Chia, L. M. L.; Rothery, J.; Watson, E. L.; McInnes, E. J. L.; Farley, R. D.; Bridgeman, A. J.; Mabbs, F. E.; Rowlands, C. C.; Halcrow, M. A. *J. Chem. Soc., Dalton Trans.* **1999**, 2087.

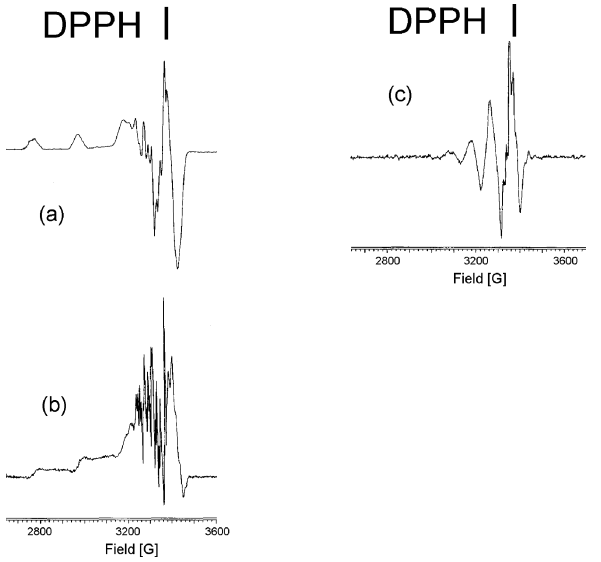

Figure 7. Temperature-dependent X-band EPR spectra of **2SiCu** in CH_2Cl_2. (a) First and (b) second derivative at $T = 100$ K. (c) Second derivative at $T = 298$ K.

with a Cu^{II}/Tl^{I} mixed-metal species (see above) and the lability of $\mathbf{1Cu_2{\cdot}(PF_6)_2}$ in most solvents with the exception of DMF. Moreover, because of electrode poisoning effects, we did not succeed in counting the number of electrons involved in any of the individual redox processes by controlled potential coulometry. We therefore refrain from a description of the cyclic voltammograms obtained.

EPR Spectroscopic Studies on the Electron-Transfer Processes. Because of the possible ambiguity between ligand-centered and metal-centered redox processes, it is useful to support the electrochemical data with EPR spectroscopic measurements on the products electrogenerated in the different anodic processes. Figure 7a,b shows the X-band EPR spectra exhibited by **2SiCu** in CH_2Cl_2 solution under glassy conditions ($T = 100$ K). A line shape analysis can be suitably carried out in terms of the $S = {}^1/_2$ electron spin Hamiltonian, resolved in the hyperfine (hpf) Cu^{II} signals (^{63}Cu, natural abundance = 69%, $I = {}^3/_2$; ^{65}Cu, natural abundance = 31%, $I = {}^3/_2$).[23−25] The signal is rather complex in that there are two partially overlapping anisotropic absorptions (relative intensities about 1:3), which exhibit resolved axial structures (in both cases $g_{\parallel} > g_{\perp} \neq g_{\text{electron}} = 2.0023$). The separation between the parallel hpf signals of the two Cu^{II} species is well evident in the first low-field absorption. Even though the resonances are rather broad, our line shape analysis supports the crystallographic result that the Cu^{II} ion in **2SiCu** is coordinated by two nitrogen and two oxygen donors in a plane (high field superposition of the two anisotropic spectral regions).[23−26] Interestingly, the narrowest high-field hpf line in the $g_{\parallel}$ region ($m_I = +{}^3/_2$ transition) exhibits superhyperfine (shpf) resolution and appears as a quintuplet signal (first and second derivative) due to coupling with the two nitrogen nuclei (^{14}N, $I = 1$). The shpf signals are somewhat broadened suggesting a slight magnetic inequivalence of the N atoms probably caused by a deviation of the ligand sphere from a strictly square planar (SQ) geometry (cf. the dihedral angle between the O(1)/Cu/N(1) and O(2)/Cu/N(2) planes of **2SiCu** is 14.8° in the solid state).[23−25,27] The relevant anisotropic parameters are collected in Table 3 together with those of the other complexes studied. At the glassy-fluid transition ($T = 198$ K), the axial features of the Cu^{II} moiety collapse such that an isotropic spectrum is obtained (Figure 7c; for more details on the EPR spectra of **2SiCu** at the glassy-fluid transition and of neat **2SiCu** under solid-state conditions see the Supporting Information). Upon oxidation of **2SiCu**, the EPR signal progressively decreases affording an X-band EPR silent species.

Figure 8 shows the low temperature ($T = 105$ K) X-band EPR spectrum of the electrogenerated cation $[\mathbf{2SiNi}]^+$ in CH_2Cl_2 solution. The $S = {}^1/_2$ line shape shows a well-defined rhombic spectrum ($g_i \neq g_{\text{electron}} = 2.0023$) with no indication of an underlying ^{61}Ni hpf structure (^{61}Ni, natural abundance = 1.2%). The g_{iso} parameters (Table 3) agree with those of similar paramagnetic Ni^{II} complexes in which the odd electron is mainly ligand centered (reduced $\delta g_{l/h} = g_l - g_h = 0.051(8)$). However, the SOMO exhibits some metal contribution as testified by the g_{iso} values, which differ significantly from those of the electrogenerated $[\mathbf{2Si}]^+$ radical (see below) as well as from the g_{iso} value of the free electron.[28] The multiple derivative line shape analysis (carried out on the intermediate and high field narrower absorptions, second and third derivative mode) indicates the presence of two almost overlapping signals. The absence of hpf and shpf splittings ($\Delta H_{\text{iso}} \geq a_{\text{iso}}(^{14}\text{N}, {}^1\text{H})$) is likely due to the effective delocalization of the $S = {}^1/_2$ unpaired electron along the overall ligand framework.[23−25,28] At the glassy-fluid transition, the rhombic pattern drops out, and the corresponding isotropic signal appears. Accordingly, the line shape is poorly resolved in the limit of the experimental line width as a consequence of both the delocalization of the unpaired electron ($\Delta H_{\text{iso}} = 8(1)$ G $\geq a_{\text{iso}}(^{14}\text{N}, {}^1\text{H})$) and the presence of the two above-mentioned overlapping paramagnetic species, detected in the third derivative. The g_{iso} and the $\langle \mathbf{g} \rangle$ values are in good agreement with each other, indicating that also in this case the primary geometry is maintained in different experimental conditions ($a_{\text{iso}} \leq \Delta H_{\text{iso}} = 8$ G). Upon rapid refreezing, the original anisotropic signals are only partially recovered because the monocation is not fully stable outside an inert atmosphere.

To rationalize the magnetic properties of **2SiCu** and $[\mathbf{2SiNi}]^+$, it is useful to look at the EPR parameters of the electro-oxidized ligand **2Si**. Figure 9 shows the pertinent room-temperature spectra of $[\mathbf{2Si}]^+$. The signal pattern displays narrow line shapes and features typical of an $S =$

(23) Pilbrow, J. H. *Transition Ion Electron Paramagnetic Resonance*; Clarendon Press: Oxford, 1990.
(24) Mabbs, F. E.; Collison, D. *Electron Paramagnetic Resonance of d Transition Metal Compounds*; Elsevier: New York, 1992.
(25) Drago, R. S. *Physical Methods for Chemists*; Saunders: New York, 1992.
(26) Peisach, J.; Blumberg, W. E. *Arch. Biochem. Biophys.* **1974**, *165*, 691.
(27) Bencini, A.; Gatteschi, D. *ESR Spectra of Metal Complexes of the First Transition Series in Low-Symmetry Environment*; Marcel Dekker Inc.: New York, 1982.
(28) Corsini, M.; Grigiotti, E.; Laschi, F.; Zanello, P.; Burgess, J.; Fawcett, J.; Gilani, S. R. *Collect. Czech. Chem. Commun.* **2003**, *68*, 1449.

Table 3. X-band EPR Parameters of the Complexes under Study[a]

	g_l[b]	g_m[b]	g_h[b]	δg[b]	$\langle \mathbf{g} \rangle$[b]	g_{iso}[b]	a_l[c]	a_m[c]	a_h[c]	$\langle \mathbf{a} \rangle$[c]
					2 SiCu Solid State					
$T = 298$ K	2.185	2.045	2.045	0.140	2.092		195	$\leq \Delta H_\perp$	$\leq \Delta H_\perp$	$\leq \langle \Delta \mathbf{H} \rangle$
	2.126	2.045	2.045	0.081	2.072		197	$\leq \Delta H_\perp$	$\leq \Delta H_\perp$	$\leq \langle \Delta \mathbf{H} \rangle$
$T = 105$ K	2.198	2.027	2.027	0.171	2.084		210	$\leq \Delta H_\perp$	$\leq \Delta H_\perp$	$\leq \langle \Delta \mathbf{H} \rangle$
	2.117	2.040	2.040	0.077	2.066		214	$\leq \Delta H_\perp$	$\leq \Delta H_\perp$	$\leq \langle \Delta \mathbf{H} \rangle$
					2 SiCu Solution					
	2.186	2.058	2.058	0.128	2.100	2.094	220[d]	29[d]	29[d]	93[d]
	2.171	2.058	2.058	0.123	2.096	2.087	228[d]	29[d]	29[d]	95[d]
					[**2SiNi**]$^+$					
	2.046	2.016	1.997	0.049	2.020	2.025	≤ 32	≤ 8	≤ 8	≤ 16
	2.046	2.015	1.994	0.052	2.018	2.024	≤ 32	≤ 6	≤ 5	≤ 14
					[**2Si**]$^+$					
	2.0062	2.0062	2.0062		2.0062	2.0068	≤ 14	≤ 14	≤ 14	≤ 14

[a] For both **2SiCu** in the solid state and [**2SiNi**]$^+$, the hpf/shpf interactions $a_{iso}(^{63,65}\text{Cu}, ^1\text{H}, ^{14}\text{N}) \leq \Delta H_{exptl}$; $\langle \mathbf{a} \rangle = 1/3(a_l + a_m + a_h)$; $\langle \mathbf{g} \rangle = 1/3(g_l + g_m + g_h)$. [b] ± 0.008 for **2SiCu** and [**2SiNi**]$^+$; ± 0.0008 for [**2Si**]$^+$. [c] a_{iso}, ΔH_{iso} in Gauss; a_{iso}, $\Delta H_i \pm 8$ G for **2SiCu**, ± 1 G for [**2SiNi**]$^+$ and [**2Si**]$^+$. [d] hpf splittings of Cu^{II}.

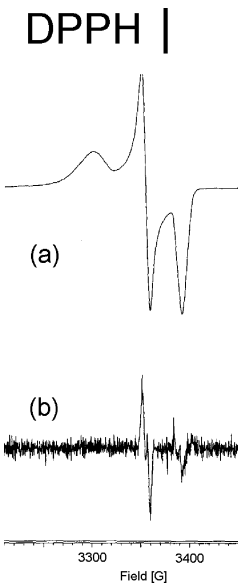

Figure 8. X-band EPR spectrum of [**2SiNi**]$^+$ in a frozen CH_2Cl_2 solution ($T = 105$ K): (a) first derivative, (b) third derivative.

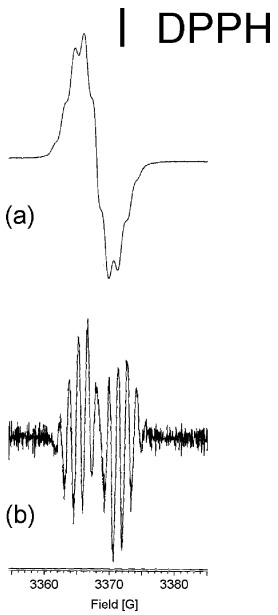

Figure 9. X-band EPR spectrum of [**2Si**]$^+$ in CH_2Cl_2 solution at $T = 298$ K: (a) first derivative, (b) third derivative.

$^1/_2$ organic radical interacting with ^{14}N and ^{1}H nuclei[23−25] ($g_{iso} \cong g_{electron}$; coupling occurs mainly to the heteroatomic linker and the aromatic rings whereas the protons of the *iso*-propyl and *tert*-butyl peripheral groups do not seem to be involved). Nine signals are detectable with a total experimental isotropic splitting of 13(1) G (low-high field peak-to-peak distance). The corresponding low-temperature spectrum displays essentially the same paramagnetic features, even though the resolution is reduced due to anisotropic line broadening effects ($g_{average} = 2.0062(8)$; total peak-to-peak distance under glassy conditions = 14(1) G; $a_{iso} \leq \Delta H_{iso} =$ 12 G).

In conclusion, the $S = {}^1/_2$ neutral complex **2SiCu** and the monocation [**2SiNi**]$^+$ exhibit different paramagnetic line shapes: The Cu^{II} complex is characterized by a noticeable metallic character as a consequence of (i) a large spin−orbit contribution to the g_{iso} values (coupling constant $\lambda < 0$), (ii) large isotropic ΔH_{iso} values typical of an $S = {}^1/_2$ $3d^9$ electronic structure, (iii) well separated and axially resolved line shapes both in the solid state and in glassy solution, and (iv) dependence of m_I on ΔH_{iso}, which is typical of low symmetry and large complexes (for example, $a_{iso} = 92$ and 97 G, respectively, for Cu^{II}; $a_{iso} = 14$ and 15 G, respectively, for ^{1}H and ^{14}N).[23−25,27] For the fact that a one-electron oxidation causes loss of the EPR signal in [**2SiCu**]$^+$, two different explanations can be envisaged: (i) the generation of a formally diamagnetic Cu(III) complex and (ii) the generation of an unpaired electron on the ligand leading to a total $S = 0$ (singlet) spin state due to antiparallel spin−spin coupling (in the presence of a total $S = 1$ (triplet) spin state, the relevant zero-field splitting features could be detectable when operating at the appropriate operational frequency; the operational frequency is about 9.5 GHz).

By contrast, in the case of [**2SiNi**]$^+$, the temperature-dependent X-band EPR features exclude a low-spin $S = {}^1/_2$ Ni(III) oxidation state for this complex, since otherwise the spectra would exhibit broad X-band signals typical of a SOMO characterized by g_{iso} values greater than $g_{electron}$ (negative spin−orbit coupling constant, $\lambda_{SO} = -715$ cm^{-1})

and significant line broadening effects as a function of temperature.[23−25,27,28] As a matter of fact, the individual lines in the actual spectra are significantly narrow, and the g_i parameters are relatively close to the value $g_{electron}$ of the free electron, indicating the SOMO of the monocation to be basically ligand centered.

UV−Vis-NIR Spectroelectrochemical Measurements. Further elucidation of the nature of the electron-transfer processes was gained through UV−vis−NIR spectroelectrochemical investigations. The electronic absorption spectrum of ligand **2Si** is dominated by a relatively intense band at $\lambda = 350$ nm. For comparison, it is noted that the well-known "salen" ligand also exhibits a main, unresolved absorption in the range $\lambda = 300-320$ nm, ascribed to $\pi \rightarrow \pi^*$ transitions involving its azomethine groups.[29,30] In the electronic spectra of salicylaldimines, a lower energy band ascribed to an $n \rightarrow \pi^*$ transition from the lone pair of the nitrogen atom to the π^* orbital associated with the azomethine groups is sometimes observed. Its eventual absence, like in the present case, indicates the existence of intramolecular hydrogen bonds connecting the hydroxyl groups to the nitrogen atoms.[29] Upon oxidation, the main spectral change is the appearance of a new band at $\lambda = 430$ nm, accompanied by the decrease of the absorption at $\lambda = 350$ nm. No intervalence charge transfer bands (IT) are detected up to $\lambda = 3300$ nm. In view of the above-mentioned spectral characteristics of salicylaldimines, we assign the new, lower energy band to the disruption of the N···H−O hydrogen bond, caused by the loss of a proton during the *p*-hydroquinone/*p*-semiquinone transition. It seems reasonable to assume that, because of conjugation with the *p*-semiquinone moiety, the π orbital of the azomethine double bond is somewhat depleted, which results in a decreased intensity of the original band at $\lambda = 350$ nm (the electronic absorption spectrum of ligand **2Si** is shown in Figure 9S of the Supporting Information, together with the spectral changes accompanying the first electron removal).

In the next step, the metal complexes **2SiCu** and **2SiNi** are to be considered. The most interesting feature observed upon their stepwise oxidation is the appearance of a very broad band in the NIR region (Figures 10 and 11). The position and broadness of these bands, together with the results of the cyclic voltammetric experiments, strongly suggest their assignment as IT transitions, thus confirming that in the electrogenerated cations [**2SiCu**]$^+$ and [**2SiNi**]$^+$ the electron is removed from the ligand, while the Cu^{II} or Ni^{II} ion merely acts as a transmitter of electronic interaction between the two redox-active halves of the ligand. Because of the cited decomposition on bulk electrolysis, only a few spectra could be collected in correspondence to the second electron removal before the isosbestic points were lost. Nevertheless, these spectra clearly show that the NIR absorption vanishes, thereby supporting the proposed assignment as an IT band. A more detailed inspection reveals three main differences between the NIR bands of [**2SiCu**]$^+$

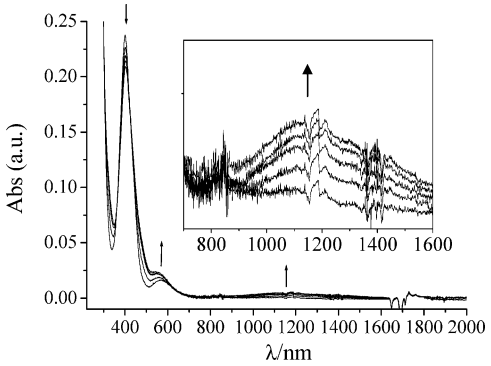

Figure 10. OTTLE cell[40] UV−vis−NIR spectra recorded on a CH_2Cl_2 solution of **2SiCu**. $[NBu_4][PF_6]$ (0.2 mol L^{-1}) was used as supporting electrolyte. Spectra were recorded after subsequent oxidation steps (initial $E_w = +0.4$ V, $\Delta E = 50$ mV, $\Delta t = 2$ min).

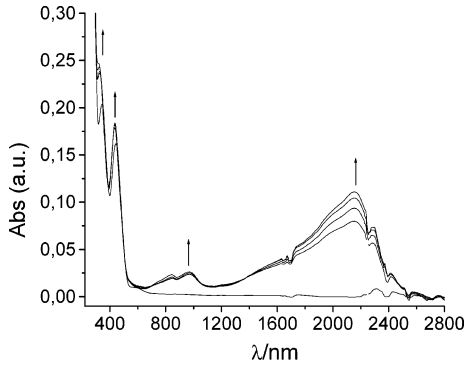

Figure 11. OTTLE cell[40] UV−vis-NIR spectra recorded on a CH_2Cl_2 solution of **2SiNi**. $[NBu_4][PF_6]$ (0.2 mol L^{-1}) was used as supporting electrolyte. Spectra were recorded after subsequent oxidation steps (initial $E_w = +0.4$ V, $\Delta E = 50$ mV, $\Delta t = 2$ min).

and [**2SiNi**]$^+$: In the first case, it is of low intensity, Gaussian-shaped, and centered at 1200 nm (8310 cm^{-1}, $\epsilon \cong 300$ M^{-1} cm^{-1}; Figure 10). In the second case, we observe a relatively intense strongly asymmetric band centered at 2155 nm (4640 cm^{-1}, $\epsilon = 3750$ M^{-1} cm^{-1}; Figure 11). Being aware of the fact that the asymmetry could be due to the presence of two or three overlapping absorptions, we will nevertheless try to extract qualitative data by preliminarily treating it as a single band. We therefore tentatively explain the differences in the NIR features of [**2SiCu**]$^+$ and [**2SiNi**]$^+$ in terms of strength of electronic coupling by using the simple two-state model. On the basis of this assumption, a picture is obtained, which is in reasonably good agreement with the results of our electrochemical investigations: The differences ($\Delta E^{\circ\prime}$) between the redox potentials of the first and the second oxidation process (Table 2) increase upon going from the free ligand **2Si** ($\Delta E^{\circ\prime} = 0.16$ V) to **2SiCu** ($\Delta E^{\circ\prime} = 0.23$ V) and **2SiNi** ($\Delta E^{\circ\prime} = 0.40$ V), suggesting that the degree of electronic interaction between the two quinoid fragments of each of these molecules increases in the same order. Because electronic coupling via the Cu^{II} ion is not very efficient, the diabatic electron transfer in **2SiCu** gives rise to a Gaussian-shaped band as predicted by the two-state treatment.[31,32] In contrast, the IT-band shape in the

(29) Bosnich, B. *J. Am. Chem. Soc.* **1968**, *90*, 627.
(30) Di Bella, S.; Fragalà, I.; Ledoux, I.; Diaz-Garcia, M. A.; Marks, T. J. *J. Am. Chem. Soc.* **1997**, *119*, 9550.
(31) Brunschwig, B. S.; Creutz, C.; Sutin, N. *Chem. Soc. Rev.* **2002**, *31*, 168.
(32) Demadis, K. D.; Hartshorn, C. M.; Meyer, T. J. *Chem. Rev.* **2001**, *101*, 2655.

spectrum of **2SiNi** is that predicted for stronger electronic coupling because it is becoming truncated on the low energy side.[31,32] The positions of the IT-band maxima are more difficult to rationalize. Indeed, for class II symmetric systems, the transition energy should remain equal to the reorganization energy required, regardless of the extent of electronic coupling. On the other side, it seems realistic to assume that such a parameter, which is mainly related to the structural differences between the *p*-semiquinone/*p*-hydroquinone redox states, should be not importantly affected by the nature of the metal. On the other side, for a class III system the optical transition is no more proportional to λ, while it becomes proportional to the electronic coupling parameter H_{ab}.[31,32] The attribution of [**2SiNi**]$^+$ to class III could explain the lower transition energy, as well as the higher intensity of its NIR band. The experimental full widths at half-height also agree with such an interpretation. In fact, for [**2SiCu**]$^+$ it results in a value much larger than the theoretical value expected as a lower limit for class II systems (7680 cm^{-1} vs 4380 cm^{-1}), while for [**2SiNi**]$^+$, under the assumption of a single band, it appears only slightly larger (3810 cm^{-1} vs 3270 cm^{-1}). Finally, the minor changes occurring in the higher energy region of the spectra give evidence that the orbital occupancy and their relative order are almost maintained, further supporting the delocalization of the charge in the cationic forms. In conclusion, while the EPR experiments definitely confirm the ligand-centered nature of the first electron removal in the case of the Ni complex, they do not disagree with the assumption that the same could be true also for the Cu^{II} complex, as supported by the spectroelectrochemical results.

Conclusion

Highly soluble square-planar Cu^{II} and Ni^{II} complexes (**2SiCu**, **2SiNi**) of siloxy-salens have been prepared in order to investigate the electronic interaction between the two *p*-hydroquinone ligands and the d^9-Cu^{II} or d^8-Ni^{II} ion. After oxidation, the positive charge in [**2SiCu**]$^+$ and [**2SiNi**]$^+$ mainly resides on the ligand, while the Cu^{II} or Ni^{II} ion merely acts as a transmitter of electronic interaction (Robin−Day[33] class II and III, respectively). According to temperature-dependent EPR spectroscopy, the singly occupied orbital (SOMO) of **2SiCu** is mainly constituted of the Cu^{II} 3d atomic orbitals. The corresponding oxidized species [**2SiCu**]$^+$ is an X-band EPR silent species, likely because the unpaired ligand-centered electron, together with the odd electron on the Cu^{II} ion, give rise to a total $S = 0$ (singlet) spin state due to antiparallel spin−spin coupling. In the case of [**2SiNi**]$^+$, the temperature-dependent X-band EPR features exclude a low-spin $S = {}^1/_2$ Ni(III) oxidation state and indicate the SOMO to be basically ligand-centered. To study also the magnetic interaction of two d^9-Cu^{II} ions via a *p*-hydroquinone bridge, we prepared the dinuclear (PMDTA)-Cu^{II} complex **1Cu$_2$·(PF$_6$)$_2$** with deprotonated 1,4-dihydroxy-2,5-bis(pyrazol-1-yl)benzene linker. X-ray crystallography revealed centrosymmetric molecules and a square-pyramidal coordination of the Cu^{II} ions with the pyrazolyl donors occupying the axial positions. The **1Cu$_2$·(PF$_6$)$_2$** compound shows the magnetic behavior of a system of isolated Cu^{II} dimers with an intradimer magnetic coupling constant of about $J/k_B = -63 \pm 5$ K. Thus, our results demonstrate the suitability of *p*-hydroquinone-based ligands as redox-active bridging units for the generation of Cu^{II}-containing oligometallic complexes and coordination polymers. We also succeeded in the preparation of a Cu^{II} coordination polymer **[1Cu]$_n$(H$_2$O)$_{2n}$** with 1,4-dihydroxy-2,5-bis(pyrazol-1-yl)-benzene bridges. However, because this particular ligand leads to unstable coordination compounds and poorly soluble materials, we are currently working on the replacement of the pyrazolyl substituents by more strongly coordinating and more solubilizing chelating sidearms.

Experimental Section

General Considerations. Instrumental Details. NMR: Bruker AMX 250, AMX 400, Bruker DPX 250. Unless stated otherwise, all NMR spectra were run at rt. ESI-MS: Fisons (now Micromass) VG Platform II. MALDI-MS: Fisons (now Micromass) VG Tofspec. TXRF: EXTRA IIA (Atomika Instruments). IR: Nicolet Magna IR 550. Quantum-Design SQUID magnetometer MPMS XL with a 5 T magnet. Materials and apparatus for electrochemistry and spectroelectrochemistry have been described elsewhere.[34,35] The complexes [Cu(PMDTA)(η^2-O$_2$CCH$_3$)]PF$_6$ and [Cu(PMDTA)(Me$_2$-CO)Cl]PF$_6$ were prepared according to a published procedure.[36] PMDTA is commercially available.

Synthesis of 1Br. 1,4-Benzoquinone (8.76 g; 81.04 mmol) and 4-bromopyrazole (11.99 g; 81.58 mmol) were suspended in 200 mL of carefully degassed ethanol. The mixture was heated to reflux for 18 h, whereupon a brown solution formed. When the solution was cooled to rt, a brown precipitate formed. The solid material was filtered off and recrystallized from hot ethanol. Yield: 2.27 g (5.67 mmol, 14%). ^{1}H NMR (d^6-DMSO, 250.1 MHz): δ 10.33 (s, 2H, OH), 8.62, 7.96 (2 × s, 2 × 2H, pz-C*H*), 7.52 (s, 2H, hqui-C*H*). ^{13}C NMR (d^6-DMSO, 62.9): δ 141.0 (hqui-CO), 140.1, 131.4 (pz-*C*H), 125.8 (hqui-CN), 111.4 (hqui-*C*H), 93.3 (pz-CBr). ESI-MS [C$_{12}$H$_8$Br$_2$N$_4$O$_2$]$^+$: $m/z = 400$. Anal. Calcd for C$_{12}$H$_8$Br$_2$N$_4$O$_2$ [400.03]: C, 36.03; H, 2.02; N, 14.01. Found: C, 35.98; H, 2.04; N, 13.78.

Synthesis of 2Si. Neat ethylenediamine (0.84 g; 14.00 mmol) was added to a solution of 2-hydroxy-3-*t*-butyl-5-(triisopropylsiloxy)benzaldehyde (9.31 g; 26.56 mmol) in 150 mL of THF. The stirred mixture was heated to reflux for 18 h and cooled to rt, and the solvent was evaporated in vacuo. The yellow oily residue was purified by column chromatography over silica gel (EtOAc/hexane 1:1). Yield: 7.91 g (10.91 mmol, 82%). Single crystals formed from an analytically pure, but still oily, sample of **2Si** upon storage at rt over a period of several weeks. ^{1}H NMR (CDCl$_3$, 250.1 MHz): δ 13.29 (s, 2H, OH), 8.28 (s, 2H, C(*H*)═N), 6.90, 6.58 (2 × d, 2 × 2H, $^4J_{HH} = 3.0$ Hz, hqui-C*H*), 3.89 (s, 4H, NCH_2), 1.39 (s, 18H, *t*Bu-CH_3), 1.18 (m, 6H, SiC*H*), 1.08 (d, 36H, *i*Pr-CH_3). ^{13}C NMR (CDCl$_3$, 62.9 MHz): δ 167.0 (*C*(H)═N), 154.6, 147.1, 138.4 (hqui-C$_{ipso}$), 122.5, 118.8 (hqui-*C*H) 118.2 (hqui-C$_{ipso}$), 59.7

(33) Robin, M. J.; Day, P. *Adv. Inorg. Chem.* **1967**, *10*, 247.
(34) Zanello, P. *Inorganic Electrochemistry. Theory, Practice and Applications*; RSC: Cambridge, 2003.
(35) Fabrizi de Biani, F.; Corsini, M.; Zanello, P.; Yao, H.; Bluhm, M. E.; Grimes, R. N. *J. Am. Chem. Soc.* **2004**, *126*, 11360.
(36) Margraf, G.; Bats, J. W.; Wagner, M.; Lerner, H.-W. *Inorg. Chim. Acta* **2005**, *358*, 1193.

(NCH_2), 34.8 (*t*Bu-*C*CH_3), 29.3 (*t*Bu-*CH*$_3$), 17.9 (*i*Pr-*CH*$_3$) 12.6 (*i*Pr-*C*CH_3). MALDI-MS $[C_{42}H_{72}N_2O_4Si_2]^+$: $m/z = 725$. Anal. Calcd for $C_{42}H_{72}N_2O_4Si_2$ [725.20]: C, 69.56; H, 10.01; N, 3.86. Found: C, 69.28; H, 9.80; N, 3.97.

Synthesis of 2SiCu. $Cu(O_2CCH_3)_2$ (0.57 g; 3.14 mmol) was added to a solution of **2Si** (2.22 g; 3.06 mmol) in 300 mL of THF. The reaction mixture was stirred for 15 h at rt. After all volatiles had been removed in vacuo, the remaining green solid was purified by column chromatography over silica gel (CH_2Cl_2/hexane 1:1). Yield: 1.49 g (1.89 mmol, 62%). Single crystals of **2SiCu** were grown from CH_2Cl_2 at −25 °C. ESI-MS $[C_{42}H_{70}CuN_2O_4Si_2]^+$: $m/z = 787$. Anal. Calcd for $C_{42}H_{70}CuN_2O_4Si_2$ [786.72]: C, 64.12; H, 8.97; N, 3.56. Found: C, 63.97; H, 9.12; N, 3.82.

Synthesis of 2Cu. A solution of **2SiCu** (1.50 g; 1.91 mmol) in 70 mL of THF was cooled to −78 °C. $[NBu_4]F{\cdot}3H_2O$ (1.21 g; 3.84 mmol) in 70 mL of THF was added dropwise with stirring under an inert gas atmosphere. The reaction mixture was allowed to warm to rt and stirred for 15 h. After addition of EtOAc (50 mL) and H_2O (50 mL), the organic layer was separated, washed with brine, and dried over $MgSO_4$. After evaporation of the solvent under reduced pressure, the remaining brown solid was dissolved in CH_2Cl_2/CH_3OH (15:1) and filtered through a short silica gel column. The green filtrate obtained was taken to dryness in vacuo. Yield: 0.83 g (1.75 mmol, 92%). MALDI-MS $[C_{24}H_{30}CuN_2O_4]^+$: $m/z = 474$. Anal. Calcd for $C_{24}H_{30}CuN_2O_4$ [474.06]: C, 60.81; H, 6.38; N, 5.91. Found: C, 60.67; H, 6.44; N, 5.71.

Synthesis of 3Cu. Neat ethylenediamine (0.33 g; 5.50 mmol) was added to a suspension of 2,5-dihydroxybenzaldehyde (1.50 g; 10.86 mmol) and $Cu(O_2CCH_3)_2$ (1.00 g; 5.51 mmol) in 200 mL of THF. The reaction mixture was heated to reflux for 18 h whereupon a brown precipitate formed. The insoluble material was isolated by filtration, triturated with CH_3OH and Et_2O, and dried in vacuo. Yield: 1.04 g (2.87 mmol, 53%). Single crystals of **3Cu**·DMF were grown from DMF at rt. MALDI-MS $[C_{16}H_{14}CuN_2O_4]^+$: $m/z = 362$. Anal. Calcd for $C_{16}H_{14}CuN_2O_4$ [361.84] × C_3H_7NO [73.09]: C, 52.47; H, 4.87; N, 9.66. Found: C, 52.34; H, 4.95; N, 9.46.

Synthesis of 2SiNi. Neat $Ni(O_2CCH_3)_2$ (0.42 g; 2.38 mmol) was added to a solution of **2Si** (1.81 g; 2.50 mmol) in 100 mL of THF/CH_3OH (1:1). The reaction mixture was stirred for 15 h at rt. After evaporation of the solvent under reduced pressure, the remaining brown solid was purified by column chromatography over silica gel (CH_2Cl_2/hexane 1:1). Yield: 1.57 g (2.01 mmol, 84%). Single crystals of **2SiNi** were grown from CH_2Cl_2 at −25 °C.

^{1}H NMR ($CDCl_3$, 250.1 MHz): δ 7.36 (s, 2H, C(*H*)═N), 6.89, 6.40 (2 × d, 2 × 2H, $^4J_{HH} = 3.0$ Hz, hqui-C*H*), 3.27 (s, 4H, NCH_2), 1.35 (s, 18H, *t*Bu-CH_3), 1.15 (m, 6H, SiC*H*), 1.06 (d, 36H, *i*Pr-CH_3). ^{13}C NMR ($CDCl_3$, 62.9 MHz): δ 161.4 (*C*(H)═N), 160.4, 143.9, 141.8 (hqui-C_{ipso}), 125.8, 119.2 (hqui-*C*H) 117.1 (hqui-C_{ipso}), 58.4 (NCH_2), 35.6 (*t*Bu-*C*CH_3), 29.5 (*t*Bu-*CH*$_3$), 18.0 (*i*Pr-*CH*$_3$) 12.6 (*i*Pr-*C*CH_3). ESI-MS $[C_{42}H_{70}N_2NiO_4Si_2]^+$: $m/z = 782$. Anal. Calcd for $C_{42}H_{70}N_2NiO_4Si_2$ [781.89]: C, 64.52; H, 9.02; N, 3.58. Found: C, 64.75; H, 9.23; N, 3.78.

Synthesis of 2Ni. A solution of **2SiNi** (1.29 g; 1.65 mmol) in 70 mL of THF was cooled to −78 °C. $[NBu_4]F{\cdot}3H_2O$ (1.04 g; 3.30 mmol) in 70 mL of THF was added dropwise with stirring under an inert gas atmosphere. The reaction mixture was allowed to warm to rt and stirred for 15 h. After addition of EtOAc (50 mL) and H_2O (50 mL), the organic layer was separated, washed with brine, and dried over $MgSO_4$. After evaporation of the solvent under reduced pressure, the remaining brown solid was dissolved in CH_2Cl_2/CH_3OH (15:1), and filtered through a short silica gel column. Yield: 0.50 g (1.06 mmol, 64%). Single crystals of **2Ni**·$(MeOH)_2$ were grown from CH_3OH at 4 °C. ^{1}H NMR (d^6-acetone, 250.1 MHz): δ 7.69 (s, 2H, OH), 7.34 (s, 2H, C(*H*)═N), 6.90, 6.51 (2 × br, 2 × 2H, hqui-C*H*), 3.45 (s, 4H, NCH_2), 1.41 (s, 18H, *t*Bu-CH_3). ^{13}C NMR: Due to the low solubility of **2Ni** in all common solvents, a decent ^{13}C NMR spectrum was not obtained. MALDI-MS $[C_{24}H_{30}N_2NiO_4]^+$: $m/z = 469$. Anal. Calcd for $C_{24}H_{30}N_2NiO_4$ [469.20]: C, 61.44; H, 6.44; N, 5.97. Found: C, 61.47; H, 6.63; N, 5.83.

Synthesis of $1Cu_2{\cdot}(PF_6)_2$. To a cloudy solution of [Cu(PMDTA)-$(Me_2CO)Cl]PF_6$ (0.95 g; 2.00 mmol) and **1** (0.24 g; 1.00 mmol) in anhydrous ethanol was added TlOEt (0.50 g; 2.00 mmol) dropwise with stirring, whereupon a purple precipitate formed. The mixture was stirred for 1 h at rt. After all volatiles had been removed in vacuo, the solid residue was treated with DMF and filtered to remove TlCl. Black X-ray quality crystals were grown by gas-phase diffusion of diethyl ether into the filtrate. Yield: 0.53 g (0.53 mmol, 53%). Anal. Calcd for $C_{30}H_{54}Cu_2F_{12}N_{10}O_2P_2$ [1003.85]: C, 35.89; H, 5.42; N, 13.95. Found (selected single-crystals): C, 35.57; H, 5.21; N, 13.63.

Synthesis of $1BrCu_2{\cdot}(PF_6)_2$. The compound was synthesized similarly to $\mathbf{1Cu_2{\cdot}(PF_6)_2}$ from $[Cu(PMDTA)(Me_2CO)Cl]PF_6$ (0.35 g; 0.74 mmol), **1Br** (0.15 g; 0.37 mmol), and TlOEt (0.18 g; 0.72 mmol). Yield: 0.16 g (0.11 mmol, 30%). Anal. Calcd for $C_{30}H_{52}$-$Br_2Cu_2F_{12}N_{10}O_2P_2$ [1161.67] × 3 C_3H_7NO [73.09] × $C_4H_{10}O$ [74.12]: C, 35.49; H, 5.75; N, 12.51. Found (selected single crystals): C, 35.22; H, 5.91; N, 12.46.

Preparation of Single-Crystalline $[1Cu]_n(H_2O)_{2n}$. Our earlier efforts to prepare single crystals of $[\mathbf{1Cu}]_n$ resulted in spherulite formation,[8] which is a typical growth form for high molecular weight compounds. From these spherulites, needles of a maximum length of 100 μm could be selected (crystal data according to X-ray powder crystallography: triclinic, $P\bar{1}$, $a = 5.1723(5)$ Å, $b = 7.9587(9)$ Å, $c = 8.2298(11)$ Å, $\alpha = 118.221(6)°$, $\beta = 91.520(9)°$, $\gamma = 100.148(8)°$). For the growth of single-crystalline $[\mathbf{1Cu}]_n(H_2O)_{2n}$, $CuSO_4{\cdot}5H_2O$ (0.012 g; 0.048 mmol) and **1** (0.012 g; 0.050 mmol) were placed separately at the bottoms of the two tubes of an H-vessel and covered with concentrated aqueous ammonia. The crystal growth rate was limited by the diffusion rate through the thin horizontal tube and could be influenced by the insertion of plugs of filter paper into this tube. Under such optimized conditions, yellow-brown platelike crystals of the size 0.12 mm × 0.10 mm × 0.03 mm formed over a period of one month, which were just large enough to be suitable for an X-ray crystal structure analysis.

Crystal Structure Analyses. The single crystals were measured on a SIEMENS SMART CCD diffractometer. In all cases, repeatedly measured reflections remained stable. Numerical absorption corrections based on six indexed crystal faces gave transmission factors between 0.940 and 0.980 (**2Si**), 0.919 and 0.960 (**2SiCu**), 0.665 and 0.872 (**3Cu**·DMF), 0.861 and 0.984 (**2SiNi**), 0.646 and 0.852 ($\mathbf{1Cu_2{\cdot}(PF_6)_2}$). In the case of $\mathbf{2Ni{\cdot}}(MeOH)_2$ ($[\mathbf{1Cu}]_n(H_2O)_{2n}$), an empirical absorption correction using the program SADABS[37] gave a correction factor between 0.859 and 1.000 (0.613 and 1.000). Equivalent reflections were averaged. All structures were determined by direct methods using the program SHELXS[38] and refined on F^2 values using the program SHELXL-97.[39] Non-H atoms were generally refined with anisotropic thermal parameters. **$2Si_B$:** The isopropyl group labeled C79, C80, and C81 was found to be

(37) Sheldrick, G. M. *SADABS*; University of Göttingen: Göttingen, Germany, 2000.
(38) Sheldrick, G. M. *Acta Crystallogr., Sect. A* **1990**, *46*, 467.
(39) Sheldrick, G. M. *SHELXL-97. A Program for the Refinement of Crystal Structures*; University of Göttingen: Göttingen, Germany, 1997.
(40) Krejčik, M.; Daněk, M.; Hartl, F. *J. Electroanal. Chem.* **1991**, *317*, 179.

disordered and was refined with a split atom model (occupancy factors 0.5). Other atoms with rather large displacement parameters are C38 and C84. The disorder of these atoms was not resolved. The H atoms were geometrically positioned and treated as riding atoms. **2SiCu:** The H atoms were geometrically positioned and treated as riding atoms. The torsion angles about the C−C bonds were refined for the methyl groups. **3Cu·**DMF: The ethylene bridge was found to be disordered over two positions (occupancy factors: 0.662(8) for C1, C2 and 0.338(8) for C1′, C2′). The asymmetric unit contains a DMF solvate group, which is disordered over two positions (occupancy factors: 0.765(4) for O5, N3, C17, C18, C19 and 0.235(4) for O5′, N3′, C17′, C18′, C19′). The H atoms were geometrically positioned and refined as riding atoms. **2SiNi:** The H atoms were geometrically positioned and were treated as riding atoms. **2Ni·**$(MeOH)_2$: The H atoms of the hydroxyl groups were taken from a difference synthesis and refined with individual isotropic thermal parameters. All other H atoms were geometrically positioned and treated as riding atoms. The H atoms at C25 could not be located. **$1Cu_2·(PF_6)_2$**: The H atoms at the benzene and pyrazolyl rings were taken from a difference synthesis and were refined with individual isotropic thermal parameters. All other H atoms were geometrically positioned and were refined as riding atoms. Torsion angles about the C−C bonds were refined for the methyl groups. **$[1Cu]_n(H_2O)_{2n}$**: To solve the structure, the Cu atom was placed at the origin. The C, N, and O atoms were taken from subsequent difference Fourier syntheses. All C−H atoms were geometrically positioned and refined as riding atoms. Possible H atom positions of the water solvate molecules were taken from a difference synthesis and refined with individual isotropic thermal parameters, using an O−H distance restraint of 0.85(2) Å. The occupancy factor of the Cu atom refined to a value of 0.836(5). This leads to the conclusion that each sixth Cu atom position is unoccupied. No distortions of the structure due to the Cu vacancies were observed. CCDC reference numbers: 234667 (**2Si**), 234662 (**2SiCu**), 234664 (**3Cu·**DMF), 234666 (**2SiNi**), 234668 (**2Ni·**$(MeOH)_2$), 234670 (**$1Cu_2·(PF_6)_2$**), 217829 (**$[1Cu]_n(H_2O)_{2n}$**).

Magnetic Measurements. All measurements were carried out on purified, microcrystalline samples; a commercial Quantum-Design SQUID magnetometer was used for the process. The samples were packed in capsules which have together with the empty sample holder a temperature independent diamagnetic moment of 2.194×10^{-5} emu at a magnetic field of 1 T.

Electrochemical Measurements. All the potential values are referred to the saturated calomel electrode. Under the present experimental conditions (solvent, CH_2Cl_2; supporting electrolyte, $[NBu_4][PF_6]$; rt), the one-electron oxidation of ferrocene occurs at $E^{\circ\prime} = +0.39$ V ($\Delta E_p = 90$ mV at a scan rate of 0.2 V s^{-1}).

Acknowledgment. M.W. is grateful to the "Deutsche Forschungsgemeinschaft" (DFG) for financial support. G.M. wishes to thank the "Fonds der Chemischen Industrie" (FCI) and the "Bundesministerium für Bildung und Forschung" (BMBF) for a Ph.D. grant. P.Z. acknowledges the financial support from the University of Siena (PAR 2003).

Supporting Information Available: Reactivity screening of various mononuclear Cu^{II} complexes and deprotonating reagents toward the *p*-hydroquinone ligand **1**, spectroelectrochemical measurements on **2Si**, description of the EPR spectra of **2SiCu** in CH_2Cl_2 solution under glassy conditions as well as at the glassy-fluid transition and of neat **2SiCu** under solid-state conditions, cyclic voltammogram of **2SiNi**, description of the changes in the UV−vis−NIR spectra of **2Si** (CH_2Cl_2 solution) upon oxidation, description of the solid-state structures of **2Si**, **2SiCu**, **3Cu·**DMF, **2SiNi**, **2Ni·**$(MeOH)_2$, and X-ray crystallographic files (CIF) of **2Si**, **2SiCu**, **3Cu·**DMF, **2SiNi**, **2Ni·**$(MeOH)_2$, **$1Cu_2·(PF_6)_2$**, and **$[1Cu]_n(H_2O)_{2n}$**. This material is available free of charge via the Internet at http://pubs.acs.org.

IC051016Z